


Article

An Insight into the Projection Characteristics of the Soil-Water Retention Surface

Yun-xue Ye ¹, Wei-lie Zou ^{1,2,*} and Zhong Han ¹ 

¹ School of Civil Engineering, Wuhan University, Wuhan 430072, China; yeyunxue@whu.edu.cn (Y.-x.Y.); zhong.han@whu.edu.cn (Z.H.)

² School of Civil Engineering, Xijing University, Xi'an 710123, China

* Correspondence: zwilliam@whu.edu.cn; Tel.: +86-27-6877-2624

Received: 25 September 2018; Accepted: 17 November 2018; Published: 23 November 2018



Abstract: The soil-water retention surface (SWRS), which describes the variation of the degree of saturation (S_r) with suction (s) and void ratio (e), is of crucial importance for understanding and modeling the hydro-mechanical behavior of unsaturated soils. As a 3D surface in the S_r – e – s space, the SWRS can be projected onto the constant S_r , constant s , and constant e planes to form three different 2D projections, which is essential for establishing the SWRS and understanding its various characteristics. This paper presents a series of investigations on the various characteristics of the three SWRS projections. For the S_r – s and S_r – e relationships, (i) a tangential approximation approach is proposed to quantitatively capture their asymptotes, and (ii) a new criterion is presented to distinguish the low and high suction ranges within which these two relationships exhibit different features. On the other hand, a modified expression is introduced to better capture the characteristics of the s – e relationships. The various projection characteristics and the proposed approaches are validated using a wide set of experimental data from the literature. Studies presented in this paper are useful for the rational interpretation of the SWRS and the hydro-mechanical coupling behavior of unsaturated soils.

Keywords: unsaturated soils; soil-water retention surface; suction; projections

1. Introduction

The hydro-mechanical behavior of unsaturated soils has been a significant research topic in geotechnical engineering over the past three decades [1–11]. Traditionally, soil's hydraulic behavior is described by the soil-water retention curve (SWRC), which is the relationship between the degree of saturation S_r and the suction s . The mechanical behavior refers to the volumetric strains caused by various external stresses. Mechanical constitutive models through the use of net stress and suction cannot describe the dependence of mechanical behavior on the degree of saturation [12,13]. Similarly, hydraulic constitutive models (such as SWRC models) cannot accurately reflect the effect of stress–strain behavior on the degree of saturation [14–17]. In other words, the hydraulic behavior and mechanical behavior of unsaturated soils are inherently coupled because the volumetric change caused by external stress modifies the SWRC simultaneously [3,5] and the change in the S_r due to s also influences soil's skeleton stress and therefore the stress–strain behavior [18–24].

Recent advances in the understanding studies on the hydro-mechanical coupling behavior of unsaturated soils typically require one to incorporate the influence of volumetric strain (i.e., void ratio e) into the description of the SWRC, considering that the degree of saturation is modified by two factors: (i) the variation in the soil water (hydraulic path), and (ii) the volume change in the soil pores (mechanical path) [25–31]. Gallipoli et al. [26] extended the van Genuchten [16] SWRC equation to incorporate e by expressing the air-entry suction as a power function of e . Gallipoli et al. [26] plotted

the e – s – S_r relationship as a 3D surface (i.e., soil-water retention surface, SWRS). This SWRS model can describe the irreversible changes of degree of saturation caused by the hydraulic (i.e., wetting and drying) and mechanical (i.e., confining pressure and shearing stress) behaviors and can be effectively used in the numerical modelling of coupled flow-deformation problems. More recently, Tarantino [32] developed a SWRC model that is similar but simpler than Gallipoli et al.'s [26] model. Gallipoli [33] improved the Gallipoli et al. [26] model to predict the hysteretic response of soils during both drying and wetting cycles at constant e and compression and swelling cycles at constant s , which is virtually the projection characteristics of the SWRS. Ghasemzadeh et al. [11] established a hysteretic SWRC model based on the power function proposed by Gallipoli et al. [26].

The advantages of using the SWRS and its projections in the rational interpretation of unsaturated soils' behavior have been discussed in several studies [30,34,35]. However, detailed discussions on the projection characteristics of the SWRS on three planes (e , s , and S_r) remain outstanding in the current literature, irrespective of their significant importance. The SWRS has three different projection scenarios: projection at constant void ratio, e , and projection at constant suction, s and projection at constant degree of saturation, S_r . On the constant e plane, projections are a series of s – S_r relationships (i.e., SWRC). On the constant s plane, projections are a series of e – S_r relationships which reflect the changes in S_r due to the mechanical stress induced variation in e . In other words, the e – S_r relationships can reflect the influence of mechanical behavior on hydraulic behavior. On the constant S_r plane, projections are a series of s – e relationships indicating the dependence of mechanical behavior on hydraulic behavior. The s – S_r and e – S_r relationships are measurable using pressure plate and unsaturated triaxial tests, while the s – e relationship cannot be directly obtained.

In this study, to investigate the projection characteristics of the SWRS on the constant e , constant s , and constant S_r planes, three independent 2-D equations are formulated based on the SWRS model proposed by Gallipoli et al. [26]. The specific characteristics of the projections are discussed in detail. Modifications and improvements are also introduced with respect to (i) capturing the asymptotes and distinguishing the different behaviors in the high and low suction ranges for the s – S_r and e – S_r relationships and (ii) describing the s – e relationships.

2. Projections of the SWRS

Based on the van Genuchten [16] model, Gallipoli et al. [26] suggested Equation (1) for the SWRS:

$$S_r = \left(1 + \left(\frac{e^\psi s}{\omega} \right)^n \right)^{-m} \quad (1)$$

where ψ , ω , m , and n are model parameters.

An example of the SWRS is shown in Figure 1 in the form of a surface mesh (its ψ , ω , n , and m values are 34.87, 0.002, 2.56, and 0.19) along with three specific projection curves obtained at $s = 200$ kPa, $e = 0.78$, and $S_r = 0.80$, respectively.

Three projection planes of the SWRS are succinctly described for providing background of how they can be used to describe the hydro-mechanical behavior of unsaturated soils:

- (i) The SWRCs: the S_r versus s plot at constant e (referred to as plane e).
- (ii) The S_r versus e plot where s is constant (referred as plane s). It is denoted as the hydro-mechanical coupling curves (HMCCs) in this paper.
- (iii) The s versus e plot at constant S_r (referred to as plane S_r). It is commonly referred to as the retention consolidation curves (RCCs).

The three projection planes were investigated using experimental data from the literature. Gallipoli [33] rewrote Equation (1) to Equation (2) in a logarithmic format.

$$\log S_r = mn \log \omega - mn\psi \log e - mn \log s + m \log \left(1 - S_r^{\frac{1}{m}} \right) \quad (2)$$

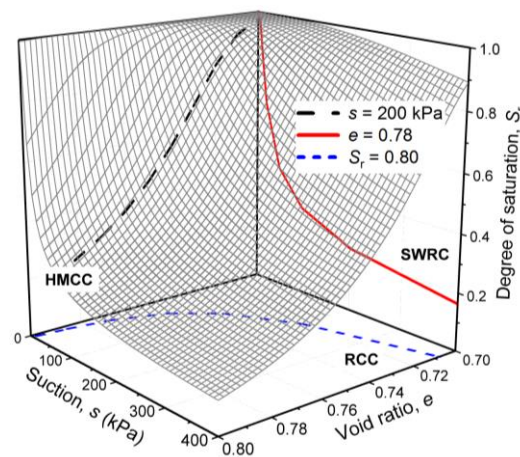


Figure 1. Schematic diagram of the three projection planes during drying.

Based on Equation (2), some interesting observations are derived from Gallipoli [33]:

(i) For the main drying path, Equation (2) on the plane e (i.e., S_r versus s plot; SWRC) has an increasing negative tangent with decreasing S_r (defined in Equation (3) and shown in Figure 2a using data from Salager et al. [36]), and the tangent is equal to $-mn$ (note that $mn > 0$) as S_r tends to zero. Similarly, Equation (2) on the plane s (i.e., S_r versus e plot; HMCC) has an increasing positive tangent with decreasing S_r and the tangent is equal to $-mn\psi$ (note that $mn\psi > 0$) as S_r tends to zero (defined in Equation (4) and Figure 2b);

$$\frac{\partial \log S_r}{\partial \log s} = -mn \left(1 - S_r^{\frac{1}{m}}\right) \quad (3)$$

$$\frac{\partial \log S_r}{\partial \log e} = -mn\psi \left(1 - S_r^{\frac{1}{m}}\right) \quad (4)$$

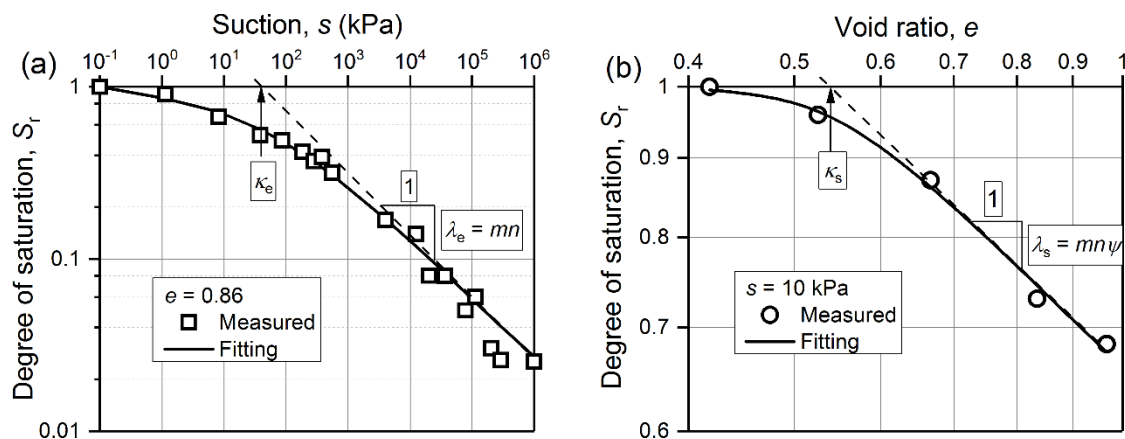


Figure 2. Main drying curves with respective asymptotes (data from Salager et al. [36]): (a) on the plane e (log-log scale), (b) on the plane s (log-log scale).

(ii) Equations (3) and (4) indicate that Equation (2) tends towards a planar asymptote in the $\log s$ – $\log e$ – $\log S_r$ space when s and e tend to infinity and S_r tends to zero. Asymptotes expression of Equation (2) was defined as Equation (5);

$$\log S_r = mn \log \omega - mn\psi \log e - mn \log s \quad (5)$$

(iii) when Equation (1) is rewritten in Equation (6) (where water ratio $e_w = eS_r$) and the product $mn\psi = 1$, the log-planar asymptote (i.e., Equation (7)) is independent of void ratio.

$$\log e_w = mn \log \omega - (mn\psi - 1) \log e - mn \log s + m \log \left(1 - S_r^{\frac{1}{m}}\right) \quad (6)$$

$$\log \bar{e}_w = mn \log \omega - (mn\psi - 1) \log e - mn \log s \quad (7)$$

Experimental data from eight soils from the published literature are used to examine the characteristics of the projections of SWRS on a logarithmic scale. Basic physical mechanical indices of these soils are summarized in Table 1.

Table 1. Summary of the index and other properties of the investigated soils.

Soil Name	w_L (%)	w_p (%)	Sand (%)	Silt (%)	Clay (%)	USCS	Reference
Silty sand	25	14.5	72	18	10	CL	Salager et al. [36]
Compacted till	35.5	16.8	28	42	30	CL	Vanapalli et al. [37]
Ca-Bentonite	99	41	n/a	n/a	n/a	CH	Sun et al. [38]
Tailing sand	n/a	n/a	30.1	55.7	14.2	ML	Aubertin et al. [39]
Sandy loam	n/a	n/a	54	35	11	SM	Laliberte et al. [40]
Sand-Bentonite	473.9	26.6	n/a	n/a	n/a	n/a	Sun & Sun [41]
Expansive Silty-Clay	50	31	3	48	39	CL	Zhan [42]
Nonexpansive-Clay	49	22	0	50	50	CL	Sun et al. [20]

Notation: n/a = not applicable.

3. Characteristics of the Projections of the SWRS

3.1. Soil-Water Retention Curves (SWRCs)

Equation (1) can be rewritten representing the plane e as below:

$$S_r = \left(1 + \left(\frac{e_0^{\psi_e} \cdot s}{\omega_e}\right)^{n_e}\right)^{-m_e} \quad (8)$$

where e_0 = initial void ratio at saturation; ψ_e , ω_e , m_e , and n_e are model parameters for plane e . Equation (8) converges to the van Genuchten [16] expression:

$$S_r = \left(1 + \left(\frac{s}{\alpha}\right)^{n_e}\right)^{-m_e} \quad (9)$$

where $\alpha = \omega_e/(e_0)^{\psi_e}$, indicating the air-entry suction; n_e is a parameter related to pore-size distribution; m_e is a parameter related to the overall symmetry of the SWRC.

Equation (5) can be rewritten as:

$$\log \bar{S}_r = m_e n_e \log \alpha - m_e n_e \log s \quad (10)$$

From Equation (10), it can be observed that (i) when $\log s$ is approaching zero; $\log \bar{S}_r$ tends to $m_e n_e \log \alpha$, and (ii) when $\log \bar{S}_r$ tends to zero; $\log s$ tends to $\log \alpha$.

SWRCs of four soils summarized in Table 1 (i.e., the silty sand, compacted till, Ca-Bentonite, and Barcelona silt) are fitted using Equation (9). Figure 3 shows an example of the SWRCs of the compacted till measured by Vanapalli et al. [37] that move towards the left-hand side along the s axis with an increasing e_0 .

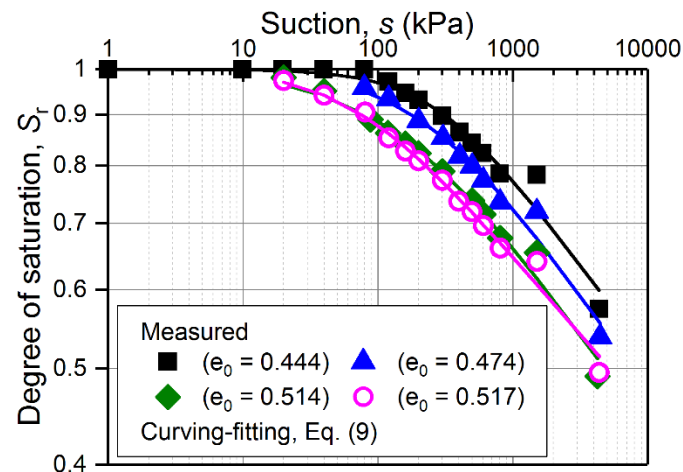


Figure 3. Main drying curves in the $\log s$ – $\log S_r$ plane (data from Vanapalli et al. [37]).

In Table 2, the values of parameters $\log \alpha$, m_e , n_e in Equation (9) and λ_e (slope of asymptotes, see Figure 2a) and κ_e (horizontal intercept of asymptotes, see Figure 2a) for the four soils at different initial void ratios are summarized. The product $m_e n_e$ is close to the absolute value of λ_e and the value of κ_e is close to $\log \alpha$. These two observations are consistent with the assumptions proposed by Gallipoli [33]. Therefore, relationships $m_e n_e \cong -\lambda_e$ and $\kappa_e = \log \alpha$ are applied in the later sections to determine the position of asymptotes.

Table 2. Values of the parameters on the plane e .

Soil Type	e_0	m_e	n_e	$\log \alpha$	κ_e	$m_e n_e$	λ_e
Silty sand (Salager et al. [36])	0.680	0.542	0.671	1.835	1.803	0.364	−0.362
	0.860	0.792	0.446	1.547	1.585	0.353	−0.364
	1.010	0.710	0.488	1.217	1.326	0.347	−0.357
Compacted till (Vanapalli et al. [37])	0.444	0.135	1.358	2.438	2.376	0.184	−0.176
	0.474	0.185	1.061	2.359	2.253	0.196	−0.184
	0.514	0.222	0.878	2.157	2.009	0.195	−0.179
	0.517	0.137	1.161	1.824	1.824	0.159	−0.158
Ca-Bentonite (Sun et al. [38])	0.940	0.253	1.162	3.135	3.138	0.293	−0.291
	1.126	0.207	1.261	2.673	2.803	0.261	−0.264
	1.765	0.213	1.271	1.969	2.040	0.271	−0.276
Tailing sand (Aubertin et al. [39])	0.695	0.809	1.116	2.025	1.905	0.904	−0.831
	0.746	0.605	1.279	1.847	1.761	0.774	−0.727
	0.802	0.479	1.272	1.655	1.598	0.609	−0.588
Sandy loam (Laliberte [40])	0.845	0.115	11.417	0.754	0.749	1.317	−1.284
	0.984	0.064	14.239	0.596	0.596	0.913	−0.913
	1.075	0.042	20.014	0.492	0.492	0.840	−0.840
	1.193	0.031	30.311	0.437	0.437	0.930	−0.930

By taking \log on both sides of the equation, $\alpha = \omega_e / (e_0)^{\psi_e}$ yields $\log \alpha = \log \omega_e - \psi_e \log e_0$. The ψ_e is the slope of the $\log \alpha$ – $\log e_0$ relationship and $\log \omega_e$ is the vertical intercept of the $\log \alpha$ – $\log e_0$ line at $\log e_0 = 0$. Figure 4 shows the $\log \alpha$ – $\log e_0$ relationships for the four soils. The results in Figure 4 are consistent with the conclusion of Stange and Horn [43], who found linear relationships between $\log e_0$ and $\log \alpha$.

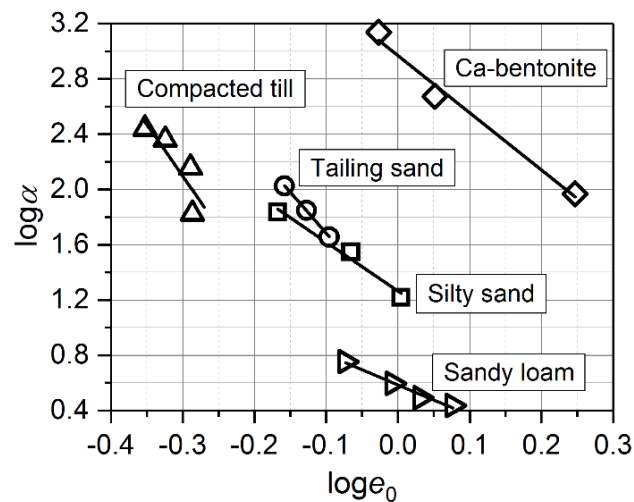


Figure 4. Linear relationship between $\log e_0$ and $\log S_r$ for five investigated soils.

Gallipoli [33] suggested that SWRCs at different initial void ratios can be obtained through a rigid translation from a reference SWRC along the s axis in the $\log s$ – $\log S_r$ plane. Similarly, HMCC at different suction can be obtained by a rigid translation from a reference HMCC along the e axis in the $\log e$ – $\log S_r$ plane. A rigid translation implies that all asymptotes of the SWRCs at different initial void ratios are parallel to each other and their $m_e n_e$ values are identical. In other words, the horizon distance between two asymptotes at different initial void ratios is constant and equals to the horizon distance between the intercepts of the two asymptotes at $\log s = 0$. This is consistent with the postulation proposed by Nuth and Laloui [28] that the SWRC has an intrinsic shape at constant e_0 and this intrinsic curve were parallel to the SWRCs at all constant values of e_0 .

In order to quantitatively capture the asymptotes, an approximate approach shown in Figure 5 is proposed. For two SWRCs with different initial void ratio e_1 and e_2 ($e_2 < e_1$), α_1 , m_1 , n_1 and α_2 , m_2 , n_2 are their parameter values of Equation (9), and λ_1 , κ_1 and λ_2 , κ_2 are the respective slope and horizontal intercept of asymptotes. Two coordinate points are required for determining the asymptotes: one point is A_1 ($\log \alpha_1$, 0) or A_2 ($\log \alpha_2$, 0) which are easily obtained; the other point can be indirectly obtained from the SWRC, referred to as matching point. According to $m_1 n_1 \cong -\lambda_1$ and $m_2 n_2 \cong -\lambda_2$, the matching point must satisfy the condition that the absolute value of the slope calculated by the two points (i.e., point A and the matching point) is close to the value of the product $m_1 n_1$ (or $m_2 n_2$). In order to obtain the matching point, an iteration-based tangential approximation method can be used, which is detailed below.

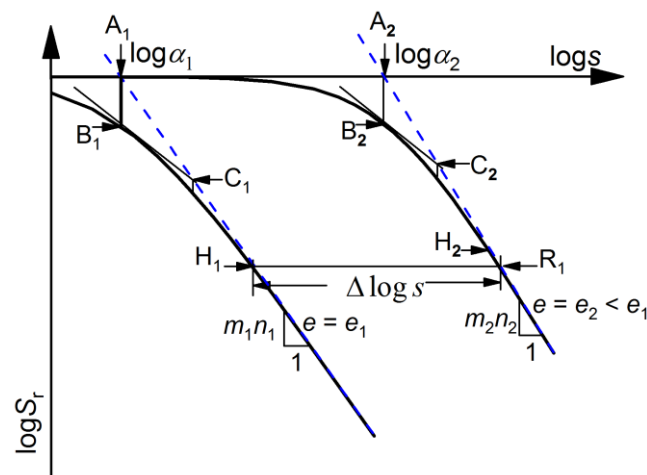


Figure 5. Main drying curves on the plane e .

Point B_1 is the vertical projection of point A_1 on the corresponding SWRC (see Figure 5). Substituting the abscissa value of point A_1 into Equation (2), point B_1 can be obtained, namely $(\log \alpha_1, m_1 \log(1/2))$. A tangent line of the SWRC at point B_1 can be conveniently defined using the slope of the SWRC defined in Equation (3) and point B_1 (i.e., $\log S_r = -1/2 \cdot m_1 n_1 \cdot (\log s - \log \alpha_1) + m_1 \log(1/2)$). With this tangent line and the asymptote of the SWRC passing point A_1 (defined by Equation (10)), point C_1 can be obtained at the intersection (see Fig 5) and its coordination is $(\log \alpha_1 - 1/n_1 \cdot \log(1/4), m_1 \log(1/4))$. The first iteration ($A_1 \rightarrow B_1 \rightarrow C_1$) ends here. Taking point C_1 as the starting point (similar to A_1), one can continue with the next iteration using the same approach detailed for first iteration. This procedure is repeated until a matching point is found. The matching point is the point where the starting point overlaps with its projection on the SWRC, and typically can be determined within seven iterations. The matching point obtained after seven iterations is denoted as point H_1 ($\log \alpha_1 + 1.5382/n_1, -1.5506m_1$). The slope calculated by both points A_1 and H_1 is about equal to $-1.008m_1n_1$, meeting the necessary condition of $m_1n_1 \cong -\lambda_1$. Therefore, the asymptotes can be well captured by points A_1 and H_1 . The proposed procedure is an objective and simple procedure to determine the asymptote. It is assumed that any points on the SWRC after point H_1 belong to the asymptote.

A simplified calibration process proposed by Gallipoli [33] was used to further validate whether the asymptote determined by points A_1 and H_1 is reasonable. The purpose of the proposed calibration is to ensure that the value of the product m_1n_1 estimated from linear best-fitting of experimental data (Equation (10)) is consistent with a logarithmic planar behavior over the experimental data range. Gallipoli [33] suggested that the values of m_1 and n_1 are considered acceptable if $\log S_r < -m_1$ over the experimental asymptotic range (m_1 and n_1 are obtained from the product m_1n_1 value using the relationship $m_1 = 1 - 1/n_1$ proposed by van Genuchten [16]); otherwise, they have to be recalibrated by imposing $\log S_{r,\max} = -m_1$, where $S_{r,\max}$ is the maximum experimental value of the degree of saturation. Considering that $\log S_r = -1.5506m_1 < -m_1$ for the matching point H_1 ($\log \alpha_1 + 1.5382/n_1, -1.5506m_1$), the asymptote computed by points A_1 and H_1 using the proposed method satisfies the criterion $\log S_r < -m_1$ suggested by Gallipoli [33] and captures the logarithmic planar behavior over the experimental range.

In order to investigate the relationship between asymptotes of two main drying curves at different values of e_1 and e_2 , the horizontal projection of point H_1 on the SWRC at e_2 can be obtained and is denoted as R_1 ($\log \alpha_2 + 1.5506m_1/m_2n_2, -1.5506m_1$). The horizontal distance between point H_1 and point R_1 in log-log scale is (see Figure 5):

$$\Delta \log s = \log \frac{\alpha_2}{\alpha_1} - \frac{1.5382m_1}{m_1n_1} + \frac{1.5506m_1}{m_2n_2} \quad (11)$$

$\Delta \log s \cong \log (\alpha_2/\alpha_1)$ when m_1n_1 is close to m_2n_2 . In this case, asymptotes of two main drying curves at different values of e_1 and e_2 are parallel. It can be seen from Table 2 that the product $m_e n_e$ of the same soil are almost the same at different values of the initial void ratio for some soils (such as silt sand, compacted till and Ca-bentonite). Therefore, their main drying curves are parallel.

The SWRCs however may not be parallel but controlled by both $m_e n_e$ and α_e , if $m_e n_e$ values are not close. An example is shown to highlight this scenario using data of a silty sand (soil properties are summarized in Table 1 and $m_e n_e$ and α_e values are summarized in Table 2). Assume its two SWRCs at $e_0 = 0.68$ and 1.01 are available and used as reference curves, while the SWRC at $e_0 = 0.86$ is used to provide comparisons between the predictions and measurements. Considering the linear relationships between $\log e_0$ and $\log \alpha$, the α value of the SWRC at $e_0 = 0.86$ can be obtained from the linear relationship defined by $\log e_0$ and $\log \alpha$ of the reference SWRCs at $e_0 = 0.68$ and 1.01 . As shown in Figure 6a, for SWRCs at $e_0 = 0.86$, the predicted curve (solid line) obtained by a rigid translation of the reference SWRC at $e_0 = 1.01$ shows better agreements with measurements than the predicted curve translated from the reference SWRC at $e_0 = 0.68$ (dash line). It can be seen from the summarized information in Table 2 that the deviation from $\log \alpha$ values of the SWRCs at $e_0 = 0.86$ to the $\log \alpha$ values of the reference SWRCs at $e_0 = 1.01$ and $e_0 = 0.68$ are 0.251 and 0.367 , respectively. This means that the

smaller deviation of $\log \alpha$ is, the higher the accuracy of the prediction is. In addition, $m_e n_e$ values of reference SWRC at $e_0 = 1.01$ are also closer to the $m_e n_e$ values of SWRC at $e_0 = 0.86$, which contributes to a better prediction.

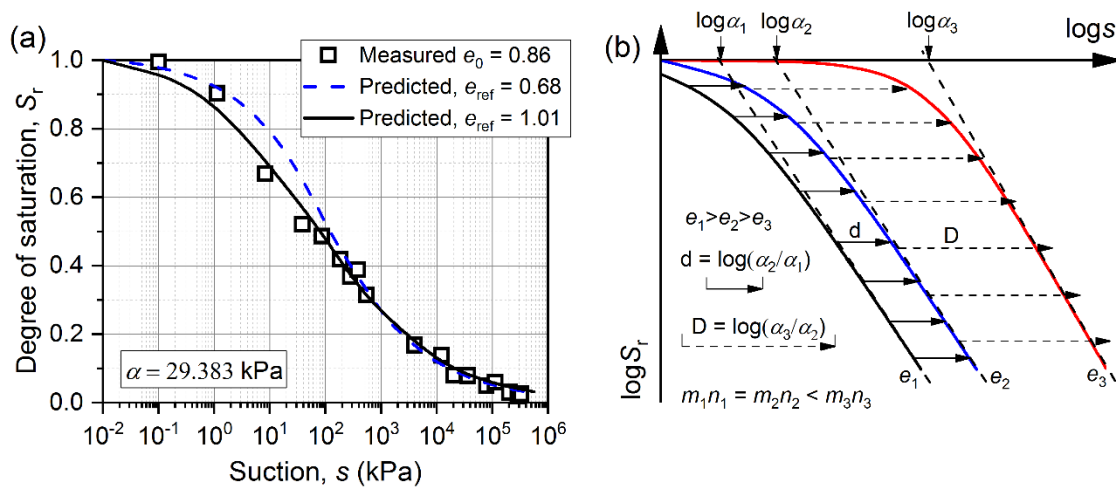


Figure 6. (a) Measured and predicted SWRC for silty sand at the initial void ratio, $e_0 = 0.86$; (b) Influence of reference SWRCs on predicted SWRCs.

In addition, Figure 6b shows three hypothetic SWRCs at e_1 , e_2 , and e_3 , respectively, for further explanation. mn values of SWRCs at e_1 and e_2 are close but different from that of SWRCs at e_3 . When mn values of two SWRCs (e.g., SWRCs at e_1 and at e_2) are close, their horizon distance d is mainly controlled by their $\log \alpha$ values. On the contrary, when mn values of two SWRCs (e.g., SWRCs at e_2 and at e_3) are different, their horizon distance D is controlled by both mn and $\log \alpha$. This is also reflected in Equation (11). The equal-length arrows in Figure 6b indicates the horizontal distance between two SWRCs can be determined by their $\log \alpha$ only (arrows with solid lines indicate shifting from SWRC at e_1 to SWRC at e_2 and arrows with dash lines indicate shifting from SWRC at e_2 to SWRC at e_3). As can be seen from Figure 6b, the horizontal shifting works well for SWRCs at e_1 and at e_2 as the arrows reach the SWRC at e_2 . On the contrary, such horizontal shifting introduces errors for SWRCs at e_2 and at e_3 as the arrows do not always stop at the SWRC at e_3 .

The products $m_e n_e$ in Table 2 are not always identical for different values of initial void ratios for some soils (such as tailing sand and sandy loam). To further validate the curve shifting method, Figure 7 shows predicted SWRCs obtained by a rigid translation of the same reference SWRC ($e_0 = 0.802$) for a tailing sand. Some differences in predictions and the measurements can be observed from the summarized information in Figure 7. These differences may be attributed to the two factors; (1) the difference in mn values, and (2) the difference in $\log \alpha$ or e_0 values. For the former, deviations in the mn values of the predicted SWRCs (at $e_0 = 0.746$ and $e_0 = 0.695$) and the reference SWRC (at $e_0 = 0.802$) are about 0.13 and 0.30 (see Table 2). Similarly, for the latter, deviations in the e values of the predicted SWRCs (at $e_0 = 0.746$ and $e_0 = 0.695$) and the reference SWRC (at $e_0 = 0.802$) are 0.056 and 0.107. Predictions using SWRC at $e_0 = 0.746$ as reference curve is slightly better than that using SWRC at $e_0 = 0.695$ as a reference curve due to the smaller deviation in the mn and e_0 values.

Another example for the sandy loam in Table 2 is shown in Figure 8. When the deviations in mn and e_0 are small, predicted SWRCs ($e_0 = 0.984$ and 1.175) obtained by a rigid translation of the same reference SWRC ($e_{ref} = 1.193$) show a good agreement with the experimental data. Therefore, three aspects deserve attention when predicting SWRCs at constant e_0 using the curve shifting method: (1) at least two sets of SWRCs with different initial void ratios experimental data must be known to estimate the parameter α values of Equation (9) and the linear relationships between $\log e_0$ and $\log \alpha$; (2) the reference curve has to be fitted by Equation (9) prior to translation because of typical limitations

of the experimental data; (3) the difference between the e_0 values of the predicted SWRCs and reference SWRCs should be as small as possible.

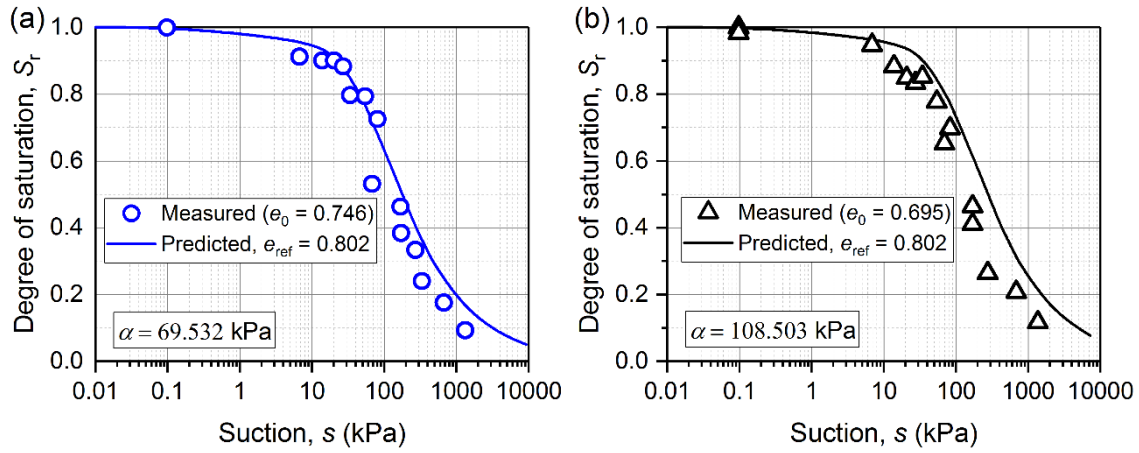


Figure 7. Measured and predicted SWRC for a tailing sand at (a) $e_0 = 0.746$; (b) $e_0 = 0.695$.

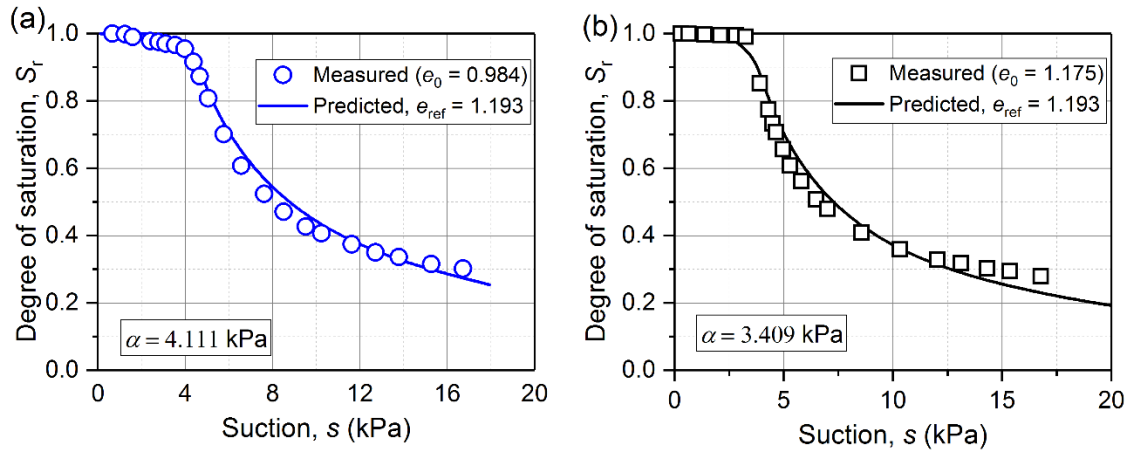


Figure 8. Measured and predicted SWRC for a sandy loam at (a) $e_0 = 0.984$; (b) $e_0 = 1.175$.

3.2. Hydro-Mechanical Coupling Curves (HMCCs)

Equation (1) is rewritten for interpreting HMCCs in the following way:

$$S_r = \left(1 + \left(\frac{e^{\psi_s} \cdot s_{con}}{\omega_s} \right)^{n_s} \right)^{-m_s} \quad (12)$$

where s_{con} = constant suction; ψ_s , ω_s , m_s , and n_s are model parameters for the constant suction condition.

Equation (5) can be rewritten as:

$$\log \overrightarrow{S_r} = m_s n_s \psi_s \log \beta - m_s n_s \psi_s \log e \quad (13)$$

where $\log \beta = \log(\omega_s / s_{con}) / \psi_s$. Equation (13) is the asymptote of Equation (2) on the plane s . When $\log e$ tends to zero, $\log S_r$ tends to $m_s n_s \psi_s \cdot \log \beta$. Meanwhile, $\log e$ tends to $\log \beta$ when $\log S_r$ tends to zero. Figure 9 shows the evolution of experimental HMCCs in $\log e - \log S_r$ plane at different constant s using data obtained from Salager et al. [36] and Sun and Sun [42]. The results indicate that HMCCs move to the left-hand side along the e axis with increasing suction.

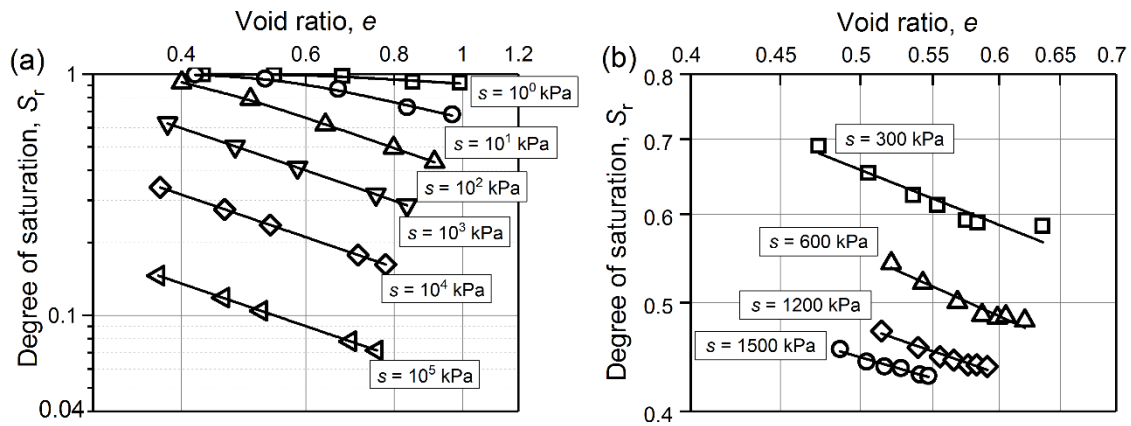


Figure 9. Hydro-mechanical coupling curves in the $\log e$ – $\log S_r$ plane: (a) resulting from hydraulic stress (data from Salager et al. [36]); (b) resulting from mechanical stress (data from Sun and Sun [41]).

The HMCCs parameters β , m_s , n_s and λ_s , κ_s for four soils used in this study at different constant suctions are summarized in Table 3. The λ_s is the slope of asymptotes and κ_s is horizontal intercept of asymptotes (see Figure 2b). It can be observed from Table 3 that: (i) the product $m_s n_s \psi_s$ is close to the absolute value of λ_s , namely $m_s n_s \psi_s \cong -\lambda_s$ and (ii) κ_s is approximately equal to $\log \beta$, namely $\log \beta \cong \kappa_s$. Note that CDG and CDE in Table 3 denote different stress paths for the constant suction, respectively. Unlike the $\log s$ – $\log \alpha$ relationships shown in Figure 4 which are linear, the $\log s_{con}$ – $\log \beta$ relationships are bi-linear.

Table 3. Values of the parameters at different values of constant suction.

Soil Type	s_{con} (kPa)	m_s (10^{-2})	n_s	$\log \beta$	$m_s n_s \psi_s$	λ_s	κ_s
Silty-Sand (Salager et al. [36])	1	0.358	7.456	−0.224	0.173	−0.173	−0.224
	10	6.65	2.383	−0.266	0.680	−0.675	−0.268
	100	11.7	2.729	−0.394	1.028	−1.027	−0.395
	1000	7.06	3.654	−0.621	1.001	−1.001	−0.621
	10,000	16.4e	4.234	−0.895	1.002	−1.002	−0.895
	100,000	33.2	1.674	−1.260	1.005	−1.005	−1.261
Sand-Bentonite (Sun & Sun [41])	300	2.68	4.446	−0.595	0.620	−0.620	−0.595
	600	6.65	2.383	−0.669	0.700	−0.669	−0.700
	1200	4.77	3.373	−0.905	0.533	−0.905	−0.533
	1500	5.66	2.643	−1.076	0.451	−0.452	−1.076
Silty-Clay (Zhan [42])	25	1.22	5.491	−0.240	0.749	−0.749	−0.240
	50	5.79	3.461	−0.284	0.786	−0.781	−0.285
	100	6.62	3.491	−0.339	0.676	−0.668	−0.341
	200	7.45	1.882	−0.390	0.625	−0.621	−0.393
Nonexpansive-Clay (Sun et al. [7])	98	1.17	3.609	−0.203	0.804	−0.804	−0.203
	147(CDG)	2.88	4.737	−0.314	0.606	−0.606	−0.314
	147(CDE)	3.42	4.716	−0.223	0.848	−0.848	−0.223
	196	2.31	2.926	−0.247	0.924	−0.924	−0.247
	245	8.49	3.017	−0.333	0.785	−0.784	−0.333

Figure 10 highlights such a relationship for silty-sand, expansive silty-clay, and a sand–bentonite mixture. These results suggest the relationship $\log \beta = \log(\omega_s/s_{con})/\psi_s$ is less effective in fitting the data over the entire suction range. Due to this reason, Equation (14) is proposed to separately describe the $\log s_{con}$ – $\log \beta$ relationships in the low and high suction ranges.

$$\log \beta_L = 1/\psi_L \cdot (\log \omega_L - \log s_L) \quad (14)$$

$$\log \beta_H = 1/\psi_H \cdot (\log \omega_H - \log s_H) \quad (15)$$

Subscripts L and H denote low suction and high suction; ψ_L , ψ_H , ω_L , ω_H , β_L , β_H are parameters. In addition, ψ_L and ω_L (or ψ_H and ω_H) have a clear physical meaning as they are associated with the slope and intercept of the straight line interpolating experimental data in the $\log s_{\text{con}} - \log \beta$ plane at low or high suctions.

To use Equation (14), it is important to distinguish low and high suction ranges. Interestingly, the asymptote (i.e., Equation (7)) is independent of the e when the product $mn\psi = 1$ in the $\log e - \log s - \log e_w$ space [33]. Tarantino [32] presented a model similar to the Gallipoli [26] expression. This model satisfies the condition of $mn\psi = 1$, and the precondition for this model is that the suction has to be located in the high suction range. Therefore, constant suctions imposed on the HMCC can be considered as high suctions when the product $m_s n_s \psi_s = 1$. It is important to note that the product $m_s n_s \psi_s$ is not always equal to 1 (see Table 3, for instance the case for the sand-bentonite and expansive silty-clay). For this reason, the imposed constant suctions will be regarded as low suctions when $0 < mn\psi < 1$. Combining with this conclusion and several sets of data related to silty sand (i.e., s_{con} and $\log \beta$) in Table 3, a bilinear relationship exists in the $\log s_{\text{con}} - \log \beta$ plane over the full suction range (see Figure 10a). It is evident for the tested silty sand that 100 kPa can be considered as the critical suction value for distinguishing low suctions from high suctions. This conclusion is consistent with the results of Salager et al. [34,36] obtained from a graphical approach that above 100 kPa suction, SWRCs with different initial void ratios can be regarded as an overlapping curve on the constant e plane. Figure 10b shows that there is a well-defined linear relationship between $\log s_{\text{con}}$ and $\log \beta$ at low suctions for sand-bentonite and expansive silty clay.

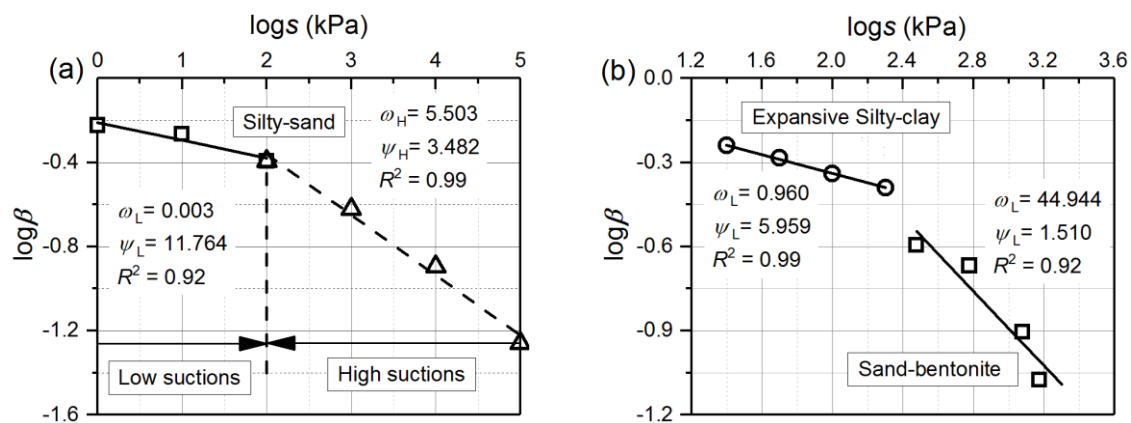


Figure 10. Linear relationship between in the $\log s - \log e$ plane at constant suction with data from Table 3: (a) at full suction range; (b) at low suctions.

For some soils, it is likely that the value of $m_s n_s \psi_s$ departs significantly from the absolute value of λ_s . A novel method is suggested in the present study to assure $m_s n_s \psi_s \cong -\lambda_s$:

(i) When $m_s n_s \psi_s > 1$ and not equal to $-\lambda_s$, $m_s n_s \psi_s$ is assumed equal to 1 and relationship $m_s = 1/(n_s \psi_s)$ is substituted into Equation (12) to fit the experimental data. This results in a new set of m_s , n_s , and ψ_s values. If the new product $m_s n_s \psi_s$ is close to $-\lambda_s$, then the m_s , n_s , and ψ_s values are deemed suitable. If still $m_s n_s \psi_s$ significantly departs from $-\lambda_s$, additional calibration is needed. In this case, the new m_s , n_s , and ψ_s values are used to plot the HMCC and the λ_s of the plotted HMCC is determined (this updated λ_s is denoted as λ_s^*). Substitute relationship $m_s = \lambda_s^*/(n_s \psi_s)$ into Equation (12) again to update m_s , n_s , and ψ_s values until $m_s n_s \psi_s \cong -\lambda_s$ is achieved. The final m_s , n_s , and ψ_s values satisfying $m_s n_s \psi_s \cong -\lambda_s$ are deemed acceptable.

(ii) When $0 < m_s n_s \psi_s < 1$ and $m_s n_s \psi_s \neq -\lambda_s$, as a first step it is assumed equal to $-\lambda_s$ and then substituted into Equation (12). The subsequent processing is the same as for the $m_s n_s \psi_s > 1$ case, which was detailed in the earlier step (i).

The advantage of this method is that both low suctions and high suctions can be clearly distinguished by the values of the product $m_s n_s \psi_s$. The product $m_s n_s \psi_s$ is approximately equal

to $-\lambda_s$ after three iterations for the data of Table 3 (bold fonts). In addition, Equation (12) with new parameter values provides a good match with experimental data. Hence, the calibration method proposed in this paper is reasonable.

Figure 11 shows a schematic diagram of the HMCCs with different constant suction values at low suctions and high suctions. Among them, $m_i n_i \psi_i$ and $\log \beta_i$ are the parameter values of Equation (13) corresponding to different constant suctions s_i ($i = 1, 2, 3, 4$). Dash lines stand for asymptotes of HMCCs (solid lines) on a logarithmic scale. All HMCCs at high suctions (i.e., $m_s n_s \psi_s = 1$) can be obtained by a rigid translation of the same graph in the $\log e$ – $\log S_r$ plane [33]. On the contrary, the values of the product $m_s n_s \psi_s$ at low suctions ($0 < m_s n_s \psi_s < 1$) are different. Due to this reason, HMCCs at high suctions may not be obtained by extending this rigid translation technique from a reference HMCC at low suctions. In other words, rigid translation is only feasible in high suction range or in low suction range, separately. Rigid translation from high suction range to low suction range or vice versa is not reliable. Figure 12 shows predicted HMCCs (at $s = 10^4$ kPa and 10^5 kPa) obtained by a rigid translation of two reference HMCCs ($s_{\text{ref}} = 10^3$ kPa and 10 kPa) for a silty sand. The translation between the prediction HMCC and the reference HMCC is evaluated by term: $|\log \beta_{\text{ref}} - \log \beta_{\text{pre}}| = |\log(s_{\text{pre}}/s_{\text{ref}})/\psi|$. The values of ψ can be obtained by Equation (14) and (15), where $\log \beta_i$ and s_i are given in Table 3 ($\psi_L = 0.085$ and $\psi_H = 0.320$). It is evident that using the reference HMCC at low suctions to predict HMCCs at high suctions can lead to deviations that are significant from the experimental data.

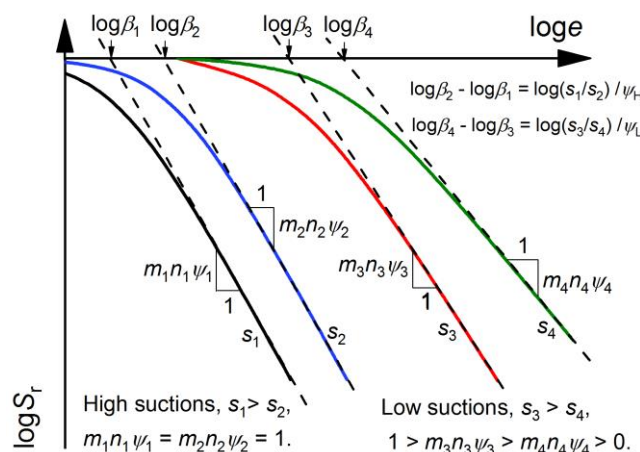


Figure 11. Schematic diagram of the hydro-mechanical coupling curves (HMCCs) with different constant suctions at low suctions and high suctions.

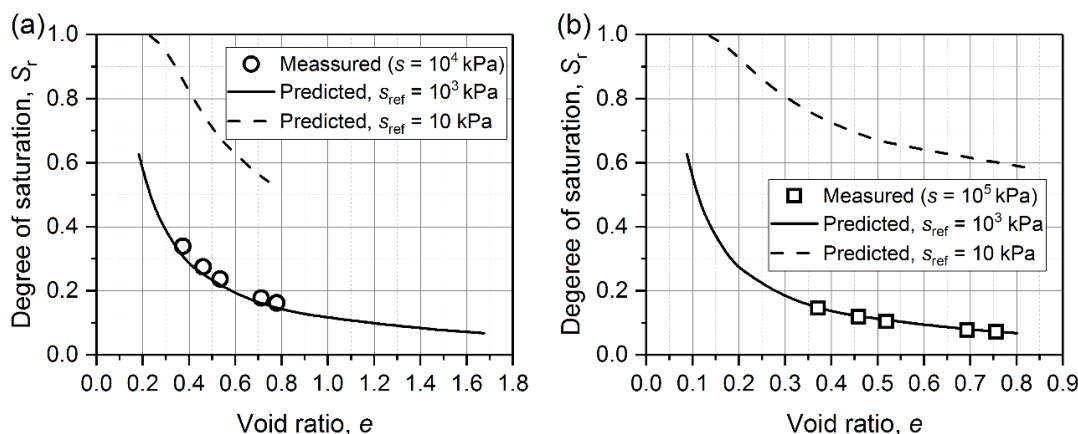


Figure 12. Measured and predicted HMCCs for a silty sand at (a) $s = 10^4$ kPa; (b) $s = 10^5$ kPa.

The method of tangential approximation described in the SWRCs section was followed to investigate the relationship between asymptotes of two main drying curves at different values of s_1 and s_2 . For a given pair of low suction values of s_1' and s_2' ($s_2' < s_1'$), the constant horizontal distance between the two asymptotes is presented in Equation (16):

$$\Delta \log e = \log \frac{\beta_2'}{\beta_1'} - \frac{1.5382m_1'}{m_1'n_1'\psi_1'} + \frac{1.5506m_1'}{m_2'n_2'\psi_2'} \quad (16)$$

where $\omega_1', \psi_1', m_1', n_1'$ and $\omega_2', \psi_2', m_2', n_2'$ are two sets of parameter values of Equation (12) corresponding to HMCCs at s_1 and s_2 , respectively. $\beta_1' = (\omega_1'/s_1)^{1/\psi_1'}$ and $\beta_2' = (\omega_2'/s_2)^{1/\psi_2'}$. $\Delta \log e$ can be considered approximately equal to $\log(\beta_2'/\beta_1')$ when $m_1'n_1'\psi_1'$ is close to $m_2'n_2'\psi_2'$. To simplify and facilitate the application, it is convenient to assume that $\omega_1' = \omega_2' = \omega_L$ and $\psi_1' = \psi_2' = \psi_L$ for low suction ranges, the horizontal distance between the predicted HMCC and the reference HMCC is $\Delta \log e = \log(s_1/s_2)/\psi_L$. A trial calculation method is introduced to improve prediction accuracy of the parameter ψ_s , in addition to Equation (14) which can be directly used to determine ψ_s .

The trial calculation method is explained using two sets of HMCC data for a sand bentonite that are summarized in Table 3. The data of HMCCs at $s = 300$ kPa and 600 kPa are taken as reference curves. The horizontal distance between these two reference HMCCs is $\Delta \log e = \log(600/300)/\psi_L$. Different ψ_L values can be tried to obtain the $\Delta \log e$ and therefore translate the HMCC at $s = 300$ kPa to HMCC at $s = 600$ kPa. A suitable ψ_L value is obtained when the translated HMCC at $s = 600$ kPa fits the measurements of the HMCC at $s = 600$ kPa. The HMCCs with different constant suctions obtained by a rigid translation of the reference HMCC ($s = 300$ kPa) and compared with experimental data (see Figure 13) to check validity of the proposed method. The results show predicted HMCCs obtained from the proposed method match well with experimental data. Therefore, the curve shifting method proposed by Gallipoli [33] is also feasible at low suctions.

Similarly, three aspects also need to be considered when predicting HMCCs at constant s using the curve shifting method: (1) at least two sets of HMCCs with different constant suctions test data must be known to estimate the ψ , and the trial calculation method proposed in this section to refine the ψ can be considered; (2) The reference curve needs to be fitted by Equation (12) prior to translation; (3) HMCCs in high suction range may be obtained from a rigid translation of a reference HMCC high suction range and rigid translation can also be used in the same way in the low suction range. However, HMCCs at high suctions cannot be obtained from a rigid translation of a reference HMCC at low suctions.

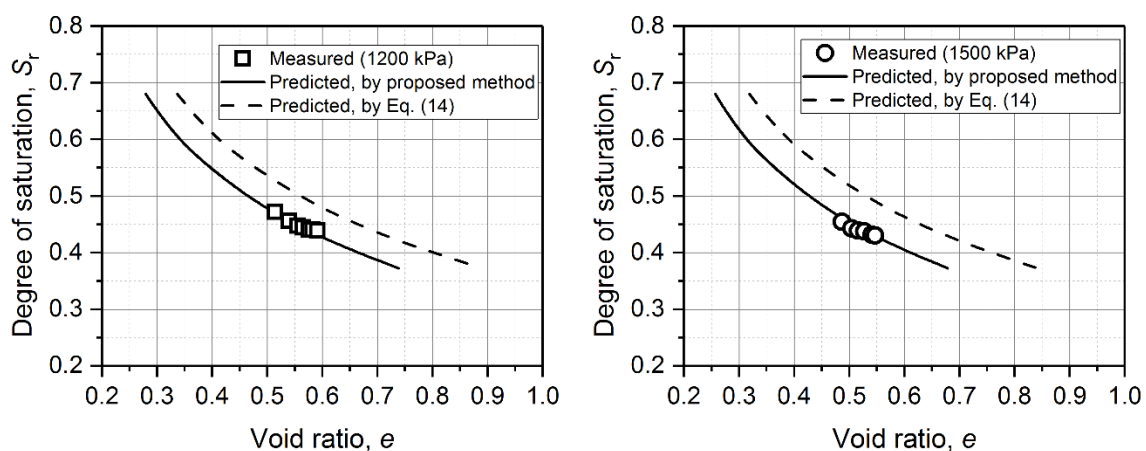


Figure 13. Measured and predicted HMCCs for sand bentonite at (a) $s = 1200$ kPa; (b) $s = 1500$ kPa.

3.3. Retention Consolidation Curves (RCCs)

Equation (1) is rewritten into Equation (17) for interpreting the RCC.

$$e = \left(\frac{\omega_{sa}}{s} \right)^{\frac{1}{\psi_{sa}}} \left(S_{rcon}^{-\frac{1}{m_{sa}}} - 1 \right)^{\frac{1}{n_{sa}\psi_{sa}}} \quad (17)$$

where S_{rcon} = constant degree of saturation; ψ_{sa} , ω_{sa} , m_{sa} , and n_{sa} are model parameters. The derivation of RCCs in the logs–log e plane at S_{rcon} is obtained as

$$\frac{\partial \log e}{\partial \log s} = -\frac{1}{\psi_{sa}} \quad (18)$$

It is difficult to measure s – e curves at constant S_r (i.e., RCC) from experimental studies. In order to represent the RCC, the SWRS (i.e., Equation (1)) shall be determined from measurements of the SWRCs at different void ratios or HMCCs at different suctions first and then set S_r to constant to obtain the RCC. Salager et al. [36] measured SWRCs of a clayey silt sand. The five sets of experimental data are fitted by Equation (1) with best-fit parameter values $\psi = 4.180$, $\omega = 11.335$, $n = 0.686$, and $m = 0.565$. RCCs at different constant S_r are obtained by substituting these parameter values into Equation (17). As shown in Figure 14, RCCs are linear in the logs–log e plane, and their slope equals to $-1/\psi_{sa}$. The RCCs move towards the left-hand direction along the s axis with the increase in constant S_r .

It should be noted that void ratio calculated from Equation (17) may exceed 1 at low suction levels, which is erroneous (see Figure 14a). On the other hand, specimens after compaction are typically unsaturated and have different initial suction levels. RCCs in Figure 14a should start from the initial suction and degree of saturation after compaction rather than from saturated condition (which is $S_r = 1$ and $s = 0.1$ kPa in Figure 14a).

Salager et al. [34] presented a relationship (Equation (19)) between the void ratio and suction using five sets of experimental data.

$$\frac{e}{e_0} = (1 - \chi) + \left\{ 1 - \frac{\ln[1 + (s/a_1)]}{\ln[1 + (10^6/a_1)]} \right\} \times \frac{\chi}{\{\ln[2.718 + (s/b_1)^{c_1}]\}^{d_1}} \quad (19)$$

where a_1 , b_1 , c_1 , d_1 , and χ are empirical parameters. The values of a_1 , b_1 , c_1 , d_1 , and χ are 1000, 400, 0.466, 2.896, and 0.21, respectively, which was suggested by Salager et al. [34].

For a saturated specimen with e_0 , its initial suctions and corresponding void ratios at different constant S_r can be obtained from the simultaneous solution of Equation (17) and Equation (19). As a result, these initial suctions and corresponding void ratios would form a curve, which is called the modified curve in this study. As shown in Figure 14b, the short-dashed line is a modified curve that shows initial states of unsaturated soil specimens at different constant S_r . The modified curve shows that the initial suction is increasing with the reducing constant S_r . For different e_0 (i.e., 0.44, 0.68, and 1.01) in Figure 14b, the initial suction is decreasing as e_0 increases at equal S_r . Such a behavior is expected because at equal S_r , the water content is increasing as initial void ratio increases based on $S_r = G_s w / e_0$, resulting in the decrease of suction. Hence, modified curves proposed in this study are reasonable.

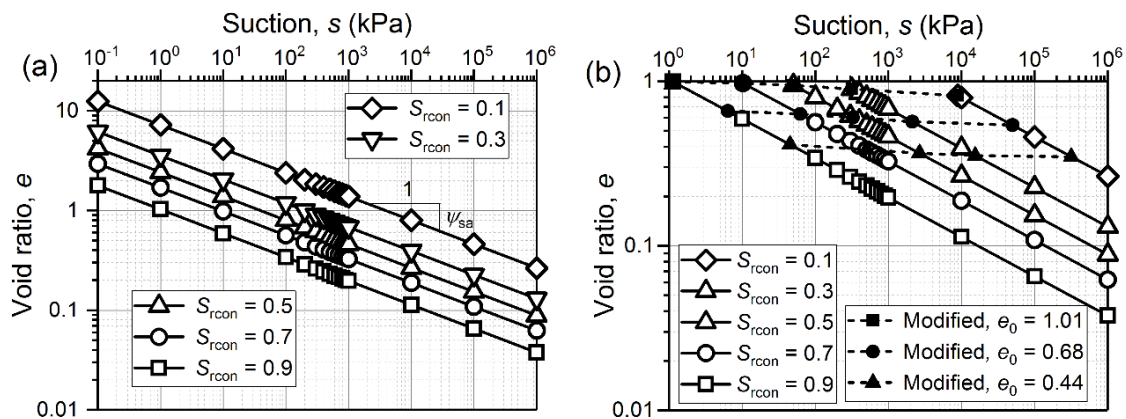


Figure 14. Retention consolidation curves at different constant degree of saturation at (data from Salager et al. [36]): (a) initial void ratio $e_0 = 0.44$; (b) different initial void ratios along with modifying lines.

4. Conclusions

Based on the SWRS model of Gallipoli et al. [26], three independent 2-D equations were presented in this paper and used to investigate the projection characteristics of the SWRS on the constant e , s , and S_r planes in order to have an insight into the hydromechanical behavior of unsaturated soils. The details are summarized below:

- (1) The SWRCs tend to move towards the left-hand direction along the s axis on a log-log scale with the increase in initial e . When the gap of initial e values between the predicted SWRCs and reference SWRCs is as small as possible, SWRCs at different initial e can be obtained by a rigid translation of a reference SWRC along the s axis in the $\log s$ - $\log S_r$ plane.
- (2) Similarly, the HMCCs and the RCCs move towards the left-hand direction along the e axis on a log-log scale with the increase in s and S_r , respectively. HMCCs at high suctions cannot be obtained from a rigid translation of a reference HMCC at low suctions. The constant suctions imposed on the HMCCs are suggested to be high suctions when the $mn\psi = 1$ and low suctions when $0 < mn\psi < 1$ (i.e., m , n , and ψ are the Gallipoli et al. [26] model parameters).
- (3) The RCC equation proposed is capable of describing the relationship between e and s on the constant S_r plane. The modified RCCs show that the initial suction increases with the reducing constant S_r . Moreover, the initial suction is reducing as initial e increases at equal values of S_r .

Author Contributions: Conceptualization, W.Z.; writing—original draft preparation, Y.Y.; writing—review and editing, W.Z. and Z.H.; supervision, W.Z. and Z.H.; funding acquisition, W.Z. and Z.H.

Funding: This research was funded by the National Natural Science Fund of China (No. 51479148 and 51809199).

Conflicts of Interest: The authors declare no conflict of interest.

References

1. Alonso, E.E.; Gens, A.; Josa, A. A constitutive model for partially saturated soils. *Geotechnique* **1990**, *40*, 405–430. [\[CrossRef\]](#)
2. Vaunat, J.; Romero, E.; Jommi, C. An elastoplastic hydromechanical model for unsaturated soils. In *International Workshop on Unsaturated Soils: Experimental Evidence and Theoretical Approaches in Unsaturated Soils*; Tarantino, A., Mancuso, C., Eds.; Springer: Balkema, Rotterdam, 2000; pp. 121–138.
3. Wheeler, S.; Sharma, R.; Buisson, M. Coupling of hydraulic hysteresis and stress-strain behavior in unsaturated soils. *Geotechnique* **2003**, *53*, 41–53. [\[CrossRef\]](#)
4. Khalili, N.; Habte, M.; Zargarbashi, S. A fully coupled flow deformation model for cyclic analysis of unsaturated soils including hydraulic and mechanical hystereses. *Comput. Geotech.* **2008**, *35*, 872–889. [\[CrossRef\]](#)

5. Gens, A. Soil–environment interactions in geotechnical engineering. *Geotechnique* **2010**, *60*, 3–74. [[CrossRef](#)]
6. Sheng, D.C.; Zhou, A.N. Coupling hydraulic with mechanical models for unsaturated soils. *Can. Geotech. J.* **2011**, *48*, 826–840. [[CrossRef](#)]
7. Sun, D.A.; Cui, H.B.; Matsuoka, H.; Sheng, D.C. A three-dimensional elastoplastic model for unsaturated compacted soils with hydraulic hysteresis. *Soils Found.* **2007**, *47*, 253–264. [[CrossRef](#)]
8. Fuentes, W.; Triantafyllidis, T. Hydro-mechanical hypoplastic models for unsaturated soils under isotropic stress conditions. *Comput. Geotech.* **2013**, *51*, 72–82. [[CrossRef](#)]
9. Masin, D. Double structure hydromechanical coupling formalism and a model for unsaturated expansive clays. *Eng. Geol.* **2013**, *165*, 73–88. [[CrossRef](#)]
10. Gao, Y.; Sun, D.A.; Zhou, A.N. Hydro-mechanical behaviour of unsaturated soil with different specimen preparations. *Can. Geotech. J.* **2016**, *53*, 909–917. [[CrossRef](#)]
11. Ghasemzadeh, H.; Sojoudi, M.H.; Amiri, S.A.G.; Karami, M.H. Elastoplastic model for hydro-mechanical behavior of unsaturated soils. *Soils Found.* **2017**, *57*, 371–383. [[CrossRef](#)]
12. Wheeler, S.; Sivakumar, V. An elasto-plastic critical state framework for unsaturated soils. *Géotechnique* **1995**, *45*, 35–53. [[CrossRef](#)]
13. Cui, Y.; Delage, P. Yielding and plastic behaviour of an unsaturated compacted silt. *Geotechnique* **1996**, *46*, 291–311. [[CrossRef](#)]
14. Gardner, W.R. Some steady state solutions of the unsaturated moisture flow equation with application to evaporation from a water-table. *Soil Sci.* **1958**, *85*, 228–232. [[CrossRef](#)]
15. Brooks, R.H.; Corey, A.T. *Hydraulic Properties of Porous Media*; Colorado State University: Fort Collins, CO, USA, 1964.
16. Van Genuchten, M.T. A closed-form equation for predicting the hydraulic conductivity of unsaturated soil. *Soil Sci. Soc. Am. J.* **1980**, *44*, 892–898. [[CrossRef](#)]
17. Fredlund, D.G.; Xing, A.Q. Equations for the soil-water characteristic curve. *Can. Geotech. J.* **1994**, *31*, 521–532. [[CrossRef](#)]
18. Ng, C.W.W.; Pang, Y.W. Influence of stress state on soil-water characteristics and slope stability. *J. Geotech. Geoenviron.* **2000**, *126*, 157–166. [[CrossRef](#)]
19. Assouline, S. Modeling the relationship between soil bulk density and the water retention curve. *Vadose Zone J.* **2006**, *5*, 554–562. [[CrossRef](#)]
20. Sun, D.A.; Sheng, D.C.; Xu, Y.F. Collapse behaviour of unsaturated compacted soil with different initial densities. *Can. Geotech. J.* **2007**, *44*, 673–686. [[CrossRef](#)]
21. Miller, G.A.; Khoury, C.N.; Muraleetharan, K.K.; Liu, C.; Kibbey, T.C.G. Effects of soil skeleton deformations on hysteretic soil water characteristic curves: Experiments and simulations. *Water Resour. Res.* **2008**, *44*. [[CrossRef](#)]
22. Masin, D. Predicting the dependency of a degree of saturation on void ratio and suction using effective stress principle for unsaturated soils. *Int. J. Numer. Anal. Methods Geomech.* **2010**, *34*, 73–90. [[CrossRef](#)]
23. Zhou, A.N.; Sheng, D.; Carter, J.P. Modelling the effect of initial density on soil-water characteristic curves. *Geotechnique* **2012**, *62*, 669–680. [[CrossRef](#)]
24. Han, Z.; Vanapalli, S.K.; Zou, W.L. Integrated approaches for predicting soil-water characteristic curve and resilient modulus of compacted fine-grained subgrade soils. *Can. Geotech. J.* **2017**, *54*, 646–663. [[CrossRef](#)]
25. Huang, S.; Barbour, S.L.; Fredlund, D.G. Development and verification of a coefficient of permeability function for a deformable unsaturated soil. *Can. Geotech. J.* **1998**, *35*, 411–425. [[CrossRef](#)]
26. Gallipoli, D.; Wheeler, S.; Karstunen, M. Modelling the variation of degree of saturation in a deformable unsaturated soil. *Geotechnique* **2003**, *53*, 105–112. [[CrossRef](#)]
27. Thu, T.M.; Rahardjo, H.; Leong, E.C. Elastoplastic model for unsaturated soil with incorporation of the soil-water characteristic curve. *Can. Geotech. J.* **2007**, *44*, 67–77. [[CrossRef](#)]
28. Nuth, M.; Laloui, L. Advances in modelling hysteretic water retention curve in deformable soils. *Comput. Geotech.* **2008**, *35*, 835–844. [[CrossRef](#)]
29. Karube, D.; Kawai, K. The role of pore water in the mechanical behaviour of unsaturated soils. *Geotech. Geol. Eng.* **2001**, *19*, 211–241. [[CrossRef](#)]
30. Tsiamposi, A.; Zdravkovic, L.; Potts, D.M. A three-dimensional hysteretic soil-water retention curve. *Geotechnique* **2013**, *63*, 155–164. [[CrossRef](#)]

31. Pasha, A.Y.; Khoshghalb, A.; Khalili, N. Hysteretic model for the evolution of water retention curve with void ratio. *J. Eng. Mech.* **2017**, *143*, 04017030. [[CrossRef](#)]
32. Tarantino, A. A water retention model for deformable soils. *Geotechnique* **2009**, *59*, 751–762. [[CrossRef](#)]
33. Gallipoli, D. A hysteretic soil-water retention model accounting for cyclic variations of suction and void ratio. *Geotechnique* **2012**, *62*, 605–616. [[CrossRef](#)]
34. Salager, S.; Ei Youssoufi, M.S.; Saix, C. Definition and experimental determination of a soil-water retention surface. *Can. Geotech. J.* **2010**, *47*, 609–622. [[CrossRef](#)]
35. Qi, S.; Simms, P.H.; Vanapalli, S.K. Piecewise-linear formulation of coupled large-strain consolidation and unsaturated flow i: Model development and implementation. *J. Geotech. Geoenviron.* **2017**, *143*, 1–11. [[CrossRef](#)]
36. Salager, S.; El Youssoufi, M.S.; Saix, C. Experimental study of the water retention curve as a function of void ratio. In Proceedings of the International Conference Geo-Denver, Denver, CO, USA, 18–21 February 2007.
37. Vanapalli, S.K.; Pufahl, D.E.; Fredlund, D.G. The influence of soil structure and stress history on the soil-water characteristic of a compacted till. *Geotechnique* **1999**, *49*, 143–159. [[CrossRef](#)]
38. Sun, W.J.; Liu, S.; Sun, D.; Fang, L.; Zhou, A. *Hydraulic and Mechanical Behavior of GMZ Ca-Bentonite*; Geotechnical Special Publication: Reston, VA, USA, 2014; pp. 125–134.
39. Aubertin, M.; Ricard, J.F.; Chapuis, R.P. A predictive model for the water retention curve: Application to tailings from hard-rock mines. *Can. Geotech. J.* **1998**, *35*, 55–69. [[CrossRef](#)]
40. Laliberte, G.E.; Corey, A.T.; Brooks, R.H. *Properties of Unsaturated Porous Media*; Hydrology Paper No. 17; Colorado State University: Fort Collins, CO, USA, 1996.
41. Sun, W.J.; Sun, D. Coupled modelling of hydro-mechanical behaviour of unsaturated compacted expansive soils. *Int. J. Numer. Anal. Methods Geomech.* **2012**, *36*, 1002–1022. [[CrossRef](#)]
42. Zhan, L. Field and laboratory study of an unsaturated expansive soil associated with rain-induced slope instability. Ph.D. Thesis, Hong Kong University of Science and Technology, Hong Kong, China, 2003.
43. Stange, C.F.; Horn, R. Modeling the soil water retention curve for conditions of variable porosity. *Vadose Zone J.* **2005**, *4*, 602–613. [[CrossRef](#)]



© 2018 by the authors. Licensee MDPI, Basel, Switzerland. This article is an open access article distributed under the terms and conditions of the Creative Commons Attribution (CC BY) license (<http://creativecommons.org/licenses/by/4.0/>).